




Stereochemical identification of glucans by a donor–acceptor–donor conjugated pentamer enables multi-carbohydrate anatomical mapping in plant tissues

Ferdinand X. Choong · Linda Lantz · Hamid Shirani · Anette Schulz ·
K. Peter. R. Nilsson · Ulrica Edlund · Agneta Richter-Dahlfors 

Received: 9 October 2018 / Accepted: 14 March 2019 / Published online: 21 March 2019
© The Author(s) 2019

Abstract Optotracing is a novel method for analytical imaging of carbohydrates in plant and microbial tissues. This optical method applies structure-responsive oligothiophenes as molecular fluorophores emitting unique optical signatures when bound to polysaccharides. Herein, we apply CarbotraceTM680, a short length anionic oligothiophene with a central heterocyclic benzodithiazole (BTD) motif, to probe for different glucans. The donor–acceptor–donor type electronic structure of CarbotraceTM680 provides improved spectral properties compared to oligothiophenes due to the possibility of intramolecular charge-transfer transition to the BTD motif. This enables differentiation of glucans based on the glycosidic linkage stereochemistry. Thus α -configured starch is

readily differentiated from β -configured cellulose. The versatility of optotracing is demonstrated by dynamic monitoring of thermo-induced starch remodelling, shown in parallel by spectrophotometry and microscopy of starch granules. Imaging of CarbotraceTM680 bound to multiple glucans in plant tissues provided direct identification of their physical locations, revealing the spatial relationship between structural (cellulose) and storage (starch) glucans at sub-cellular scale. Our work forms the basis for the development of superior optotracers for sensitive detection of polysaccharides. Our non-destructive method for anatomical mapping of glucans in biomass will serve as an enabling technology for developments towards efficient use of plant-derived materials and biomass.

Electronic supplementary material The online version of this article (<https://doi.org/10.1007/s10570-019-02381-5>) contains supplementary material, which is available to authorized users.

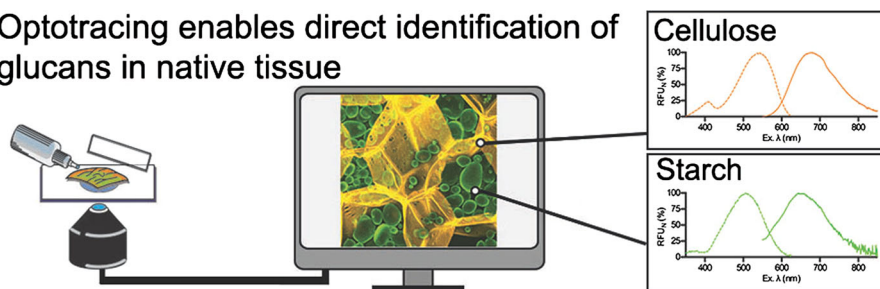
F. X. Choong · A. Schulz · A. Richter-Dahlfors (✉)
Swedish Medical Nanoscience Center, Department of
Neuroscience, Karolinska Institutet,
SE-171 77 Stockholm, Sweden
e-mail: agneta.richter.dahlfors@ki.se

L. Lantz · H. Shirani · K. Peter. R. Nilsson
Department of Chemistry, IFM, Linköping University,
SE-581 83 Linköping, Sweden

U. Edlund
Fibre and Polymer Technology, KTH Royal Institute of
Technology, SE-100 44 Stockholm, Sweden

Graphical abstract

Optotracing enables direct identification of glucans in native tissue



Keywords Cellulose · Starch · Glucose polysaccharides · Optotracing · Non-disruptive carbohydrate analysis

Introduction

In our societies strive to replace fossil materials by plant derived alternatives, new and improved low-cost/high-efficiency methods for composition determination and extraction process monitoring are required (Galkin et al. 2017). Plants serve as an abundant and renewable source of polysaccharides, which are materials with a wide range of applications. Pulp from Sweden's forestry industry supports a quarter of EU's total demand in which cellulose is the most important component (Heinsoo 2017). In the food and beverage industry, polysaccharides such as alginate and starch are extensively used as stabilizers and gelling agents (Tasneem et al. 2014). In pharmaceuticals, alginate, starch, cellulose and their combinations have been proposed as ideal materials for biocompatible drug carriers (Wang et al. 2010). Cellulose derivatives are excessively used drug excipient binders and coating agents (Sheskey et al. 2017). Starch and cellulose are also common precursors of biofuel. The best-suited application area(s) for a given polysaccharide is determined by the chemical and physical properties, with the stereochemistry, substitution pattern, and degree of polymerization (DP) representing key factors. Such information is however difficult to achieve, since sample preparation protocols for conventional carbohydrate analyses, such as ion chromatography, involve massive degradation of the polymer prior to analysis. Glucans, polysaccharides composed solely of glucose monomers linked by

glycosidic bonds, are exceptionally challenging to differentiate, since all information on the native stereochemistry and branching pattern is lost during sample preparation. Thus the molecular origin of the glucose residues cannot be determined. Moreover, methods able to identify and differentiate native polysaccharides from each other while preserving the architecture of the tissue are scarce (Galkin et al. 2017; Barnette et al. 2011).

Optotracing was recently reported by us as a non-destructive method for material composition analysis (Choong et al. 2016a, b). The location and quantity of carbohydrates is visualised by fluorescence emitted from oligothiophenes binding to target molecules within the native sample. We showed that the structure-responsive fluorescent oligothiophenes excel as optical sensors for analytical imaging of cellulose and lignocellulosic materials. Binding via non-covalent interactions between the oligothiophene and the carbohydrate backbone induces geometric changes in the thiophene backbone, which results in ON/OFF like switching of fluorescence with unique spectral qualities. We applied a cationic optotracer in a novel spectrophotometric method for assessment of the purity of cellulose in fibres from pulp production and biomass extraction (Choong et al. 2016b). Next, we used the anionic heptameric oligothiophene h-FTAA to produce an anatomical map of cellulose in its native location in tissues of plants (Choong et al. 2018). Visualisation is based on optical detection of the cellulose specific spectral signature generated by h-FTAA aligned to $\beta(1\text{--}4)$ configured glucose with $\text{DP} \geq 8$. In contrast, shortening of the cellodextrins ($\text{DP} < 8$), chemical modifications of the hydroxyl groups, or stereochemical differences in glycosidic linkages hampered quantification of cellulose and the spectra based identification of carbohydrates in plant

tissues. Thus, some chemical requirements are essential to promote optimal non-covalent interactions with anionic optotracers and cellulose.

Optotracers of varying length differ in their binding modes (Shirani et al. 2017). This influences the reporting capability, as was demonstrated using heptameric and tetrameric oligothiophenes in detection of disease-associated protein aggregates (Klingstedt et al. 2011; Bäck et al. 2016). Shorter oligothiophenes have, however, a narrow reporting capability due to a relatively small Stokes shift and restricted fluorescent characteristics. To overcome this, we synthesized a chemically improved oligothiophene, in which the central thiophene moiety was substituted for a benzothiadiazole (BTD) motif (Shirani et al. 2015). This motif provides a donor–acceptor–donor (D–A–D)-type electronic structure, in which efficient intramolecular charge-transfer can be afforded between thiophenes as electron donors and nitrogen-containing heterocycles as effective electron acceptors. This generates a relatively large Stokes shift of the D–A–D conjugated pentamer, similar to what is observed in efficient, light harvesting materials in solar cells, in solid-state organic photovoltaic and in organic field effect transistor applications (Beaujuge et al. 2010).

Here, we hypothesize that D–A–D conjugated pentameric optotracers are sufficiently short in length to gain access to small binding sites, while at the same time provide enhanced spectral separation for improved reporting capability. Based on spectral recordings from CarbotraceTM680 we develop a simple and rapid method that differentiates glucans based on their stereochemistry. The versatility of optotracing is shown by its applicability in dynamic sensing of thermo-induced responses in starch granules, and as a fluorescent marker for spatially resolved visualization of starch and cellulose at sub-cellular scale in their natural environment in potato tissue sections. Our work establishes the new concept of analytical imaging, enabling detection of carbohydrates and their anatomical locations in native plant materials.

Experimental section

Optotracers, glucans, native starch granules and plant tissue

CarbotraceTM680 (originally reported in Shirani et al. 2015) was obtained from Ebba Biotech (Stockholm, Sweden), HS-84 was synthesized as described (Shirani et al. 2015). Stock solutions (1.40×10^{-3} mol/L) were prepared in deionised water and stored at 4 °C. Microcrystalline cellulose fibres (M. cellulose, 100 µm) from cotton liners (CAS no. 9004-34-6), laminarin from *Laminaria digitata* (CAS no. 9008-22-4), starch from corn (CAS no. 9005-25-8), amylose from potato (CAS no. 9005-82-7), amylopectin from maize (CAS no. 9037-22-3), glycogen from bovine liver (CAS no. 9005-79-2), dextran (CAS no. 9004-54-0) and sodium carboxymethyl cellulose (CAS no. 9004-32-4) with DS 0.7 and DS 1.2 respectively, wherein DS refers to the degree of substitution, were from Sigma-Aldrich (Stockholm, Sweden). Glucans were dissolved/suspended in ‘ultrapure water’ of ‘type 1’ (ISO 3693). Glucans were maintained as 2 mg/mL stock solutions at 4 °C. Potatoes (*Solanum tuberosum* L.) from local supermarkets were stored at 4 °C. Native starch granules were isolated by soaking peeled and shredded fresh potatoes in 50 mL phosphate buffered saline (PBS), pH 7.4 (Sigma-Aldrich, Stockholm, Sweden) and granules released into the supernatant were harvested by centrifugation at 5000 g for 5 min. Following one wash in 50 mL PBS, native starch granules were isolated by centrifugation. The wet mass of the pellet was measured and re-suspended into a 20 mg/mL stock in PBS for experimentation.

Optical recordings of CarbotraceTM680 and HS-84 interacting with polysaccharides

Aliquots (50 µL) of each glucan stock solution were pipetted into individual wells of a white 96-well round bottom microtiter plate (Corning, Stockholm, Sweden). Stock solutions of CarbotraceTM680 and HS-84 were diluted in PBS to a final concentration of 4.6×10^{-6} mol/L, from which 50 µL was added to each well. Samples were sealed with adhesive plate seals (Thermo-Fischer, Stockholm, Sweden), the plate was incubated at 4 °C on a rocking shaker for 30 min, then positioned in a Synergy MX plate reader (Biotek, Stockholm, Sweden). The excitation spectrum of

CarbotraceTM680 (emission at 600 nm) was collected between 300 and 580 nm and the emission spectrum (excitation at 500 nm) was collected between 520 and 850 nm. The excitation spectrum of HS-84 (emission at 600 nm) was collected between 300 and 580 nm and the emission spectrum (excitation at 450 nm) was collected between 470 and 700 nm. Spectra were collected with the ‘instruments’ ‘top-down’ setting with 1 nm steps. Data from triplicate experiments were processed and analysed using Prism 6 (Graphpad, USA).

Preparation and optical recording of cellulose nanofibrils

Cellulose nanofibrils were prepared as previously described (Biermann 1996) from bleached never-dried softwood pulp (Domsjö dissolving plus) containing 20% (w/w) dry content ($\sim 93\%$ cellulose, $\sim 5\%$ hemicellulose) by 2,2,6,6-tetramethylpiperidine-1-oxyl radical (TEMPO) oxidation (Isogai et al. 2011; Saito et al. 2007). The oxidized pulp was defibrillated by mixing, ultrasonification and mechanical stirring until a 2% (w/w) gel of nanofibrils dispersed in water was achieved. For optical recordings, the 2% (w/w) gel of nanofibrils was further diluted in PBS to a concentration of 0.57% (w/w). Aliquots (50 μ L) was then pipetted into individual wells of a 96-well round bottom microtiter plate (Sarsted, Stockholm, Sweden). 50 μ L of a 4.6×10^{-6} mol/L solution of CarbotraceTM680 was added to each well. Samples were sealed with adhesive plate seals (Thermo-Fischer, Stockholm, Sweden), the plate was incubated at 4 °C on a rocking shaker for 30 min, then positioned in a Synergy MX plate reader (Biotek, Stockholm, Sweden). The excitation spectrum of CarbotraceTM680 (emission at 600 nm) was collected between 300 and 580 nm. Spectra were collected with the ‘instruments’ ‘top-down’ setting with 1 nm steps. The data was processed and analysed using Prism 6 (Graphpad, USA).

Optical characterization of CarbotraceTM680 at different pH

The CarbotraceTM680 stock solution was diluted in 20 mM Na-citrate buffer pH 3.0, 20 mM Na-acetate buffer pH 4.0 or pH 5.0, and 20 mM Na-phosphate buffer pH 6.0 or pH 7.0 to a final concentration of

2.79×10^{-6} mol/L. Absorption- and emission spectra were recorded with an Infinite M1000 Pro microplate reader (Tecan, Männedorf, Switzerland). Data from triplicate experiments were processed and analysed using Prism 6 (Graphpad, USA).

Staining of M. cellulose and plant tissues in situ

M. cellulose was stained by soaking 1 mg in 1 mL CarbotraceTM680 (4.6×10^{-6} mol/L) in PBS for 30 min in room temperature. Unbound CarbotraceTM680 was removed by centrifugation (5000 g, 5 min), and the pellet was washed twice in PBS. Samples were mounted in a drop of mounting medium (DAKO, Stockholm, Sweden) on a microscopy slide, sealed with a glass coverslip, then analysed by multi-detector imaging and multi-laser/multi-detector analysis. Plant tissues were prepared for in situ fluorescence microscopy by cutting square tissues (10 \times 10 mm) from 1 mm thin slices of potato. Each tissue was incubated in a well of a 12-well plate (Sarstedt, Numbrecht, Germany) containing 2 mL CarbotraceTM680 (4.6×10^{-6} mol/L) in PBS. Following 30 min incubation in room temperature, tissues were washed by immersion in PBS, then mounted on microscopy slides as described above. Tissues incubated in PBS without CarbotraceTM680 served as negative control in the following imaging analysis.

Multi-laser/multi-detector analysis

In the multi-laser/multi-detector analysis, a fluorophore is excited at multiple wavelengths, while emitted fluorescence is simultaneously detected by two or more photomultiplier tubes (PMTs). We excited CarbotraceTM680 at 405 nm, 473 nm, 535 nm and 635 nm. On our confocal laser-scanning microscope (Olympus, Stockholm, Sweden), we loaded the software Fluoview FV1000 (Olympus, Stockholm, Sweden) using factory pre-sets for Alexa Fluor 405, Alexa Fluor 488, Alexa Fluor 546 and Alexa Fluor 633 and individually placed into separate ‘Groups’. Sequential acquisition in ‘Frame’ mode was selected during imaging. The resulting paired laser/PMT wavelengths were 405/430–450 nm, 473/490–540 nm, 535/575–620 nm and 635/655–755 nm (Figure S1a in the Supporting Information). To avoid pixel saturation or cut-off of emitted fluorescence, we

replaced the standardized Voltage, Gain and Offset settings by individual calibration of PMTs using the ‘High-Low’ setting. Negative controls were imaged using the same setting as for their corresponding CarbotraceTM680 stained sample. Phase contrast images were collected in the transmitted light detector with excitation at 473 nm. Images and image stacks were collected using the lenses UPLSAPO 20x NA0.75, UPLSAPO 40X 2 NA0.95 and UPLSAPO 60XW NA1.2 (Olympus, Stockholm, Sweden).

Recording of thermo-induced starch swelling and gelling

To induce swelling, 1 mL aliquots of native starch granules (10 mg/mL) stained with CarbotraceTM680 (6.98×10^{-6} mol/L) were pipetted into 1.5 mL tubes and placed into a Eppendorf[®] Thermomixer[®] (Sigma-Aldrich, Sweden). Samples were heated from 20 to 90 °C, using 10 °C steps. Each temperature was maintained for 20 min, before heating to the next temperature. At the end of each temperature incubation, 100 µL was withdrawn from each sample and pipetted into wells of a round bottom 96-well plate, which was placed in a Synergy MX plate reader (Biotek, Stockholm, Sweden). Morphological changes in the native starch granules were measured by recording the optical density of the suspension at 600 nm (OD₆₀₀). Data were analysed by plotting OD₆₀₀ against respective temperature using Prism 6 (Graphpad, USA). Additionally, each sample was analysed by an area scan in which the density of starch granules, measured as OD₆₀₀, at each of 29 points in the well were recorded. Data were analysed and presented in the form of a heat map, with red representing high and blue representing low density (Prism 6, Graphpad, USA). All experiments were performed with 3 repeats.

Excitation and emission spectra of the CarbotraceTM680 stained native starch granules at each temperature were performed by recording the excitation spectrum (emission at 600 nm) between 300 and 580 nm, and the emission spectrum (excitation at 500 nm) between 520 and 750 nm in the Synergy MX plate reader (Biotek, Stockholm, Sweden). Ex. λ_{\max} and RFU_S were determined and plotted against the respective temperature using Prism 6 (Graphpad, USA).

Once the morphological and spectral analyses were completed, contents of each well were transferred onto a glass slide and imaged by multi-laser/multi-detector analysis on a confocal laser-scanning microscope.

Preparation and analysis of images and videos

Fiji (Wisconsin, USA) was used to process image stacks into single optical projections, Z-projections, 3D projections, and videos.

Results and discussion

Optotracing for specific visualization of cellulose in materials

To determine whether a BTM motif in the central position of an optotracer (Fig. 1a) influences its ability to detect cellulose, we analysed the optical signature of CarbotraceTM680 in PBS in the absence and presence of M. cellulose. Spectral analysis showed that CarbotraceTM680 in its unbound form absorbs between 300 and 580 nm with peak excitation (Ex. λ_{\max}) at 505.5 nm (Fig. 1b). The molecule is weakly fluorescent when detected between 520 and 850 nm, with peak emission (Em. λ_{\max}) at 575.5 nm. When added to M. cellulose in PBS, the spectral characteristic of CarbotraceTM680 is markedly altered. Binding of the molecule to cellulose results in an Ex. λ_{\max} at 534.5 ± 30 nm and an Em. λ_{\max} at 677.7 ± 21.5 nm.

The significant increase in emitted fluorescence shows that the binding induced geometric shift of the optotracer backbone serves as an ON-like switch of fluorescence. Due to the effect of donor–acceptor interaction on the π -electron system (Beaujuge et al. 2010), CarbotraceTM680 displayed a two-band absorption profile with the prominence of the intramolecular charge band at the higher wavelength. Similar to previous reports on anionic optotracers, the cellulose specific emission signature from CarbotraceTM680 was abolished upon chemical modification of the hydroxyl groups on the carbohydrate backbone (Figure S1 in the Supporting Information). To identify the type of molecular geometry that is associated with the red shift, we analysed the spectra of CarbotraceTM680 in buffers ranging from pH 3 to pH 7 (Fig. 1c). We found that acidic pH (pH 3–5)

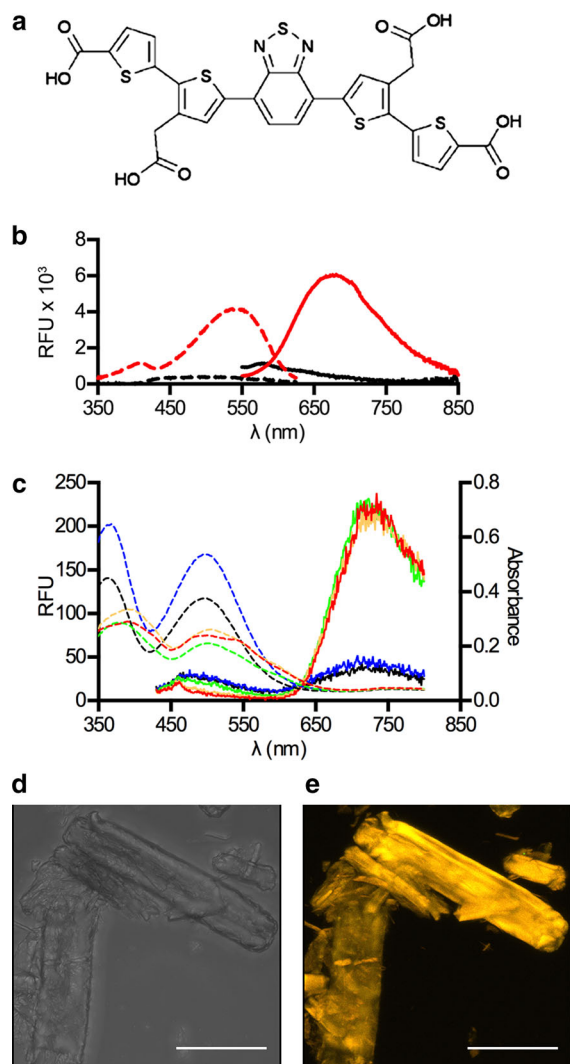


Fig. 1 Visualisation of cellulose by CarbotraceTM680. **a** Chemical structure of CarbotraceTM680 showing the central BTD motif. **b** Excitation (dashed line) and emission (solid line) spectra defines the optical signature of CarbotraceTM680 binding to M. cellulose. Emitted fluorescence from CarbotraceTM680 in PBS in the absence (black) and presence (red) of M. cellulose is plotted at each wavelength. **c** Absorbance (dashed line) and emission (solid line) spectra of CarbotraceTM680 in buffers of pH 3 (red), 4 (yellow), 5 (green), 6 (blue) and 7 (black). **d, e** Micrographs of M. cellulose fibres stained by CarbotraceTM680 shown by **d** phase contrast and **e** multi-laser/multi-detector analysis, in which stained cellulose fibres are pseudo-coloured in yellow. Micrographs represent 3D brightest point projections of image stacks (25.52 μm stack, z-step = 1.16 μm) collected by confocal microscopy. Scale bar: 50 μm . An animation of this image stack is found as Video S1 in the Supporting Information

induced a red shift of the absorption spectrum, suggesting that a conformational transition of the backbone occurs with decreasing pH and protonation of the carboxyl side chain functionalities. Moreover, the strong emission at 730 nm suggests that acidic pH induces a conformation that favours the intramolecular charge-transfer transition to the BTD motif. In contrast, the backbone adopts an alternative conformation at pH 6 and 7, as evidenced from less emission at 730 nm and increased fluorescence at 500 nm. The latter emission is associated with the π - π^* transition. Collectively, our data shows that an optotracer harbouring a central BTD motif binds cellulose and produces a spectrum with red shifted Em. λ_{max} and increased fluorescence, likely due to an efficient intramolecular charge-transfer transition to the BTD motif.

For visual confirmation of cellulose binding, we performed a multi-laser/multi-detector analysis of M. cellulose stained with CarbotraceTM680. Under phase contrast, M. cellulose was optically dense, predominantly appearing as large crystals surrounded by multiple small fragments (Fig. 1d). Sequential imaging at 405/430–450 nm, 473/490–540 nm, 535/575–620 nm and 635/655–755 nm (Figure S2a–f in the Supporting Information) revealed strong fluorescence from CarbotraceTM680 localised throughout the crystal of M. cellulose (Fig. 1e). This resulted in the emission of distinct yellow–red fluorescence when the stained crystal was excited at 535 nm and 635 nm. By stepping through the z-stack of images of CarbotraceTM680 stained M. cellulose, detailed features such as surface ridges, smooth crystal faces and smaller crystal fragments were easily visualised (Video S1 in the Supporting Information). This verifies the suitability of CarbotraceTM680 as a stain for specific visualization of cellulose in materials.

CarbotraceTM680 differentiates $\alpha(1 \rightarrow 3)$, $\alpha(1 \rightarrow 4)$, $\alpha(1 \rightarrow 6)$, $\beta(1 \rightarrow 3)$, $\beta(1 \rightarrow 4)$ and $\beta(1 \rightarrow 6)$ linked glucans at the molecular level

We predicted that short length oligomers, such as CarbotraceTM680, would have access to a wide range of binding sites, thereby increasing the range of glucans that can be detected by optotracing based on stereochemical differentiation of the glycosidic linkages. To test this hypothesis, we performed a spectral analysis of CarbotraceTM680 mixed with the β

configured glucans M. cellulose and laminarin, as well as the α configured starch, amylose, amylopectin, glycogen and dextran. The excitation and emission spectra of each mix were recorded and the Ex. λ_{\max} was determined using normalised spec-plots, a graph in which the amplitude in each excitation spectra was normalized to range between 0 and 100% (Figure S3a-h in the Supporting Information). Additionally, we calculated the relative fluorescence units across the entire spectra (RFU_s) of each mix (Figure S3i in the Supporting Information). The highest RFU_s was observed from CarbotraceTM680 bound to cellulose, whereas binding to dextran emitted low RFU_s, similar to unbound CarbotraceTM680 serving as negative control. RFUs of all other glucans ranged in-between. This suggests that CarbotraceTM680 adopts a different geometry when bound to the α -configured amylose, starch, amylopectin and glycogen as compared to its binding to cellulose. By plotting the emitted RFU_s from each CarbotraceTM680/glucan mix against the corresponding Ex. λ_{\max} , the glucans separated into groups, which at closer inspection corresponded to the glycosidic bonds of each sample (Fig. 2a). In comparison to unbound CarbotraceTM680, which has an Ex. λ_{\max} at 505.5 nm, binding to the β (1 \rightarrow 4) configured cellulose induced a large, +28.5 nm red shift in Ex. λ_{\max} . A similar, albeit less pronounced red shift (+16.5 nm) was observed in laminarin, a glucan with primarily β (1 \rightarrow 3) and β (1 \rightarrow 6) linkages. In contrast, binding to the α (1 \rightarrow 4) configured amylose induced a 10 nm decrease in Ex. λ_{\max} , while the Ex. λ_{\max} of CarbotraceTM680 bound to the remaining α -configured glucans starch, amylopectin, and glycogen were centred close to unbound CarbotraceTM680. In an attempt to further separate glucans in this cluster, we plotted Em. λ_{\max} of each sample against its corresponding Ex. λ_{\max} (Fig. 2b). Compared to unbound CarbotraceTM680, showing an Em. λ_{\max} of 575.5 nm, binding of CarbotraceTM680 to amylose, amylopectin, starch, glycogen, laminarin and cellulose induced major red shifts, to longer than 650 nm. Factoring Em. λ_{\max} into the plot magnified the differences between Ex. λ_{\max} of the glucans. This further differentiated the α (1 \rightarrow 4) configured amylose from starch, amylopectin, and glycogen, which contains α (1 \rightarrow 4) and α (1 \rightarrow 6) linkages. Based on the complete lack of change in RFU_s, Ex. λ_{\max} and Em. λ_{\max} from CarbotraceTM680 added to dextran, we conclude that the optotracer did not bind this glucan,

possibly due to lack of binding sites arising from extensive branching.

To determine whether the ability to differentiate the stereochemistry of glycosidic linkages depends on the BTD motif in CarbotraceTM680, we synthesized HS-84. This pentameric optotracer is identical to CarbotraceTM680 except for a replacement of the central BTD motif to a thiophene moiety (Fig. 2c). Experiments were performed to determine the Ex. λ_{\max} and Em. λ_{\max} for HS-84 interacting with all glucans (Figure S4a-h in the Supporting Information). When plotting Em. λ_{\max} of each sample against its corresponding Ex. λ_{\max} , cellulose showed an increase of +33.5 nm in Ex. λ_{\max} and +11 nm in Em. λ_{\max} compared to unbound HS-84 (Fig. 2d). All other glucans emitted the same optical signals as unbound HS-84. Cellulose thus represents the only glucan identifiable by HS-84. Collectively, our experiments demonstrate that a shorter length oligomer, here shown for the pentameric CarbotraceTM680, increases the range of detectable polysaccharides as compared to the heptameric optotracer we previously used for cellulose detection (Choong et al. 2016a, 2018). Moreover, introducing a central BTD motif in CarbotraceTM680 enabled a wide range of optical signatures, which is essential for the detection of multiple targets. With higher variations in the colours, wavelengths, and signal intensities, BTD-containing optotracers thus opens for the use of optical detection and differentiation of glucan stereochemistries.

Monitoring of heat-induced starch re-organisation

CarbotraceTM680 based detection of starch was remarkable, considering the striking difference between its α -configuration in comparison to the β -configured cellulose. To ensure that the starch detection did not occur as an artefact of the commercial preparation of powdered starch, we repeated the experiment using native starch granules, which we isolated from freshly shredded potato parenchyma. Spectrophotometric analysis of CarbotraceTM680 mixed with native starch granules showed Ex. λ_{\max} of 517.5 ± 16.9 and Em. λ_{\max} of 575.5 ± 18.9 nm (Fig. 3a). This corresponded to +12 nm and +90 nm red shifts respectively, compared to spectra from unbound CarbotraceTM680. A difference of approximately +12.5 nm in Ex. λ_{\max} and +75 nm in Em. λ_{\max} was observed for stained native starch

Legend

- Cellulose + Carbotrace™680 / HS-84
- △ Laminarin + Carbotrace™680 / HS-84
- Starch + Carbotrace™680 / HS-84
- ▼ Amylose + Carbotrace™680 / HS-84
- Amylopectin + Carbotrace™680 / HS-84
- Glycogen + Carbotrace™680 / HS-84
- ◇ Dextran + Carbotrace™680 / HS-84
- Carbotrace™680 / HS-84 only

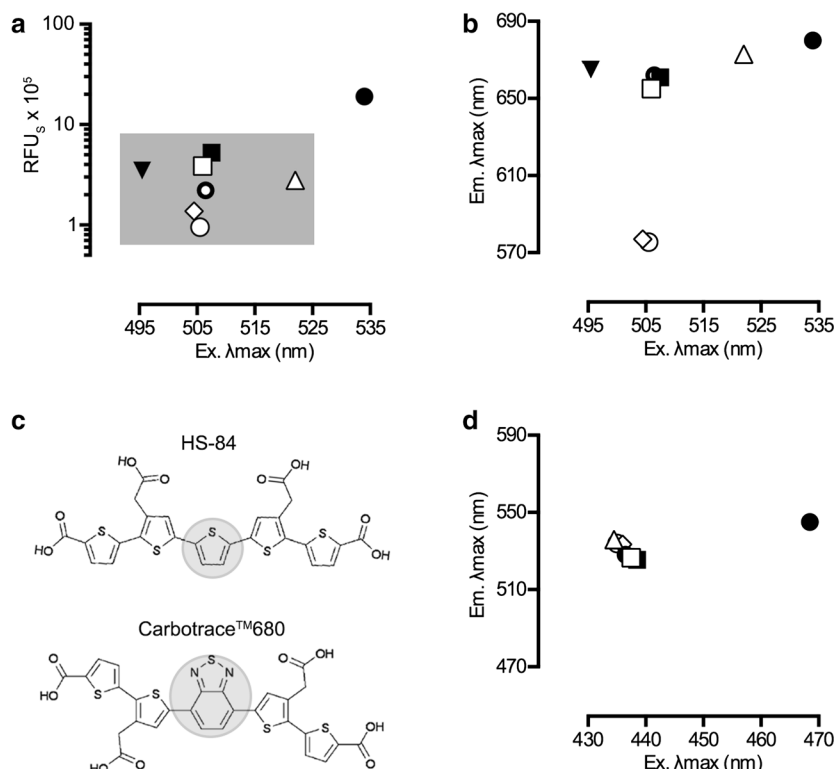


Fig. 2 Carbotrace™680 enables stereochemical differentiation of glycosidic linkages in glucans. **a** Optical signatures, defined by plotting emitted RFUs against Ex. λ_{\max} from Carbotrace™680 interacting with M. cellulose, laminarin, starch, amylose, amylopectin, glycogen and dextran. The signal from Carbotrace™680 with no added glucans is shown as negative control. Each data point represents the average from 3 independent experiments. **b** Optical signatures, defined by plotting Em. λ_{\max} against Ex. λ_{\max} for experiments shown in (a),

reveal stereochemistry-dependent clustering glucans stained by Carbotrace™680. **c** The chemical structure of HS-84 and Carbotrace™680 with their central thiophene and BTB motifs, respectively, highlighted in grey. **d** Optical signatures, defined by Em. λ_{\max} plotted against Ex. λ_{\max} from HS-84 interacting with M. cellulose, laminarin, starch, amylose, amylopectin, glycogen and dextran. The signal from HS-84 with no added glucans is shown as negative control. Each data point represents the average from 3 independent experiments

granules compared to stained powdered potato starch. These experiments show that Carbotrace™680 indeed detects starch, as well as small differences in commercial and native preparations.

We next analysed whether Carbotrace™680 can be used as a fluorescent stain to visualise the native starch granules. To obtain an initial, general overview, we applied phase contrast microscopy to Carbotrace™680 stained native starch granules. This revealed a mixed population of variously sized granules, showing different morphologies and clustering (Fig. 3b, top panel). When switching to multi-laser/multi-detector analysis of the same sample, granules appeared in bright green (Fig. 3b, bottom panel). By stepping through the z-stack of images collected on the confocal microscope, we observed the

most intense green fluorescence on the exposed surface and the outer layer of granules, decreasing towards the core. Faint striations, likely corresponding to alternating layers in crystalline and amorphous lamina, could be observed in the larger granules. Such patterned staining is likely attributed to varying rates of the diffusion of Carbotrace™680, afforded by differences in polysaccharide packing density at each lamina. Staining with Carbotrace™680 thus visualises very fine details of the morphology of native starch granules at sub-cellular scale.

Starch is a thermo-sensitive material that undergoes drastic morphological changes when heated. Having identified Carbotrace™680 as an optical sensor for starch granules, we investigated the applicability of this novel technique to dynamically monitor the

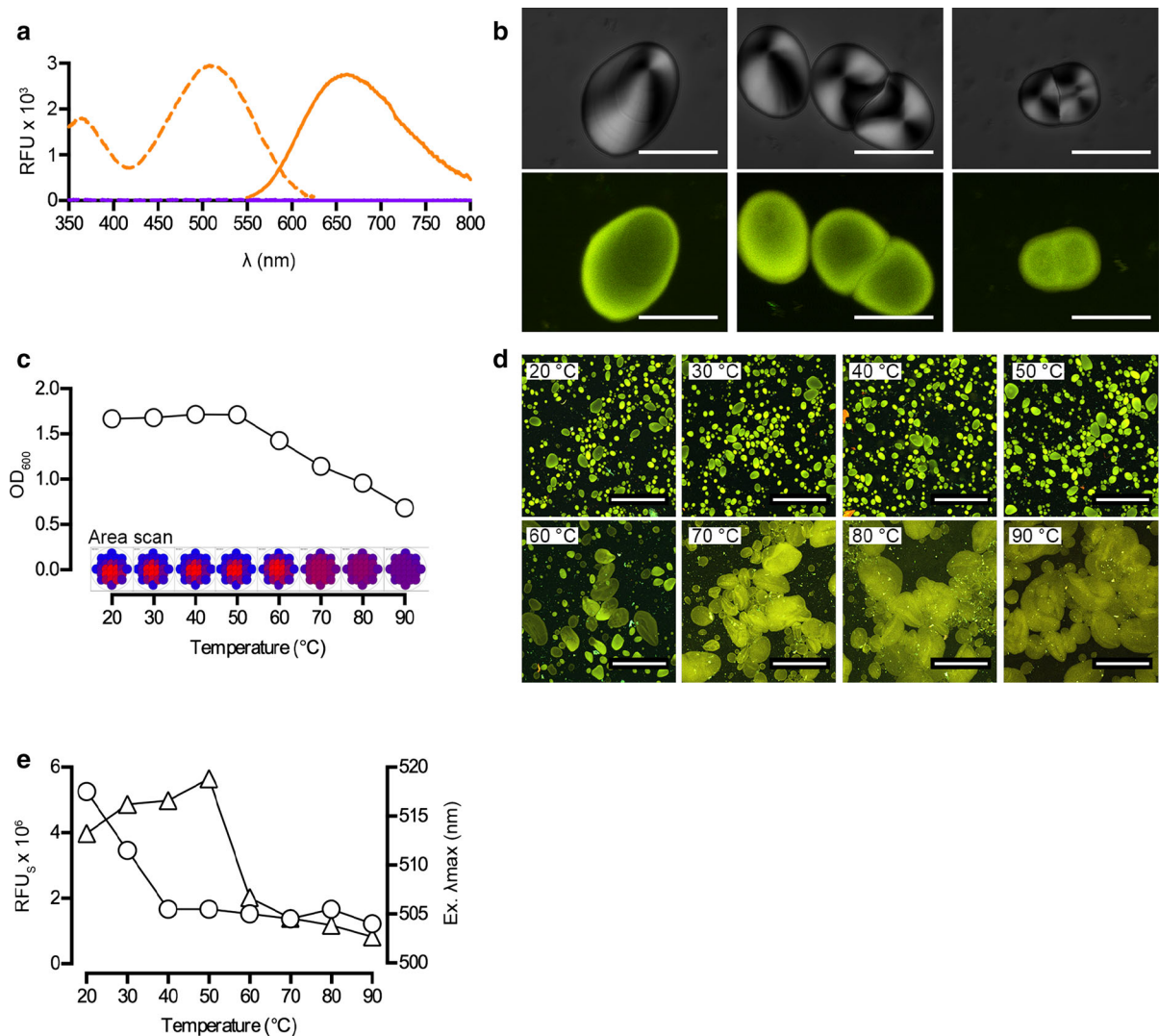


Fig. 3 Spectral and fluorescence recording of Carbotrace™680 bound to starch for visualisation of granules and kinetic monitoring of thermo-induced starch re-organisation. **a** Excitation (dashed line) and emission (solid line) spectra of Carbotrace™680 in unbound form in PBS (purple) and when bound to native starch granules (orange) from potato. Fluorescence (RFU) is plotted at each wavelength. **b** Multi-laser/multi-detector analysis of native starch granules from potato tissue stained by Carbotrace™680. A single optical plane from phase contrast (top panel) and fluorescence (lower panel) imaging show examples of common forms adopted by the granules. Scale bar = 20 μm . **c** Thermo-induced swelling of native starch

thermo-responses of starch. To study heat-induced swelling, we exposed Carbotrace™680 stained native starch granules to temperatures increasing from 20 to 90 °C at 10 °C increments, and analysed samples from each temperature in a plate reader.

granules stained with Carbotrace™680. The optical density at 600 nm is measured of granules exposed to a step-wise increase in temperature from 20 to 90 °C. Data are shown as single point measurements (solid line) and by area scans as indicated. **d** Visualisation of starch granules from (c), revealing thermo-induced swelling as temperatures increase. Images from each temperature are acquired by multi-laser/multi-detector analysis. Scale bar = 200 μm . **e** Thermo-induced swelling of starch granules defined by the optical signature of bound Carbotrace™680. Relative fluorescence units (RFU_s, triangle) and Ex. λ_{max} (circle) are plotted against the applied temperature

Spectrophotometric recordings showed that the optical density (OD₆₀₀) remained the same at 20–50 °C (Fig. 3c). At 60 °C, a sharp decrease occurred that became more prominent as the temperature reached 90 °C. The same pattern was observed when samples

were analysed by area scans. The occupied area in each well remained the same at temperatures up to 50 °C, whereas a marked increase was observed at higher temperatures. In parallel, we visualized the changing morphology by microscopy. Samples taken from each temperature were mounted onto glass slides and prepared for confocal microscopy using multi-laser/multi-detector analysis. The CarbotraceTM680 stained native starch granules showed no change in granule size and morphology when heated from 20 to 50 °C (Fig. 3d). At 60 °C, distinct swelling was observed, and further heating to 90 °C resulted in progressively larger starch granules. Thus, optical density recordings and visualization by microscopy both show that major effects on heat-induced swelling of native starch granules occur at temperatures above 50 °C.

The multi-laser/multi-detector analysis also revealed that higher temperatures induce a visible change in the fluorescence colour and intensity of CarbotraceTM680 stained starch granules (Fig. 3d). To quantify this change in fluorescence, we analysed the optical spectra of samples from each temperature. Based on the excitation and emission spectra (Figure S5a,b in the Supporting Information), we determined the RFU_S and Ex. λ_{max} , and plotted both parameters against the corresponding temperature (Fig. 3e). For RFU_S, a gradual increase was observed from 20 to 50 °C, before it dropped sharply at 60 °C. This lower level was maintained throughout the higher temperatures. This result is in accordance to the absorbance-based method identifying 60 °C as the temperature for swelling to occur (Fig. 3d). Tracking of Ex. λ_{max} showed, however, a distinctly different result. Starting from an Ex. λ_{max} of 517.5 nm at 20 °C, a distinct drop to 505 nm occurred directly when heat was applied, and this drop was arrested at 40 °C. Higher temperatures did not further influence the Ex. λ_{max} , as it held steady around 505 nm from 50 to 90 °C. Spectrophotometric definition of Ex. λ_{max} thus identifies early-stage, heat-induced starch rearrangements, long before morphological changes become visible to the eye. We propose that optical analysis of CarbotraceTM680 stained starch greatly improves the detection sensitivity of thermo-induced morphological changes, since minor rearrangements in starch packing and swelling can be identified.

Mapping the anatomical location of cellulose and starch in plant tissues

CarbotraceTM680 provides distinctly different optical signatures when bound to cellulose compared to starch, as a result from the optotracer's ability to stereochemically differentiate the two. As the optical signatures are well resolved, we analysed if CarbotraceTM680 can be used to simultaneously visualise multiple glucans within plant tissues, thereby providing an anatomical map of their physical location. We selected potato as model tissue, since the compartmentalized location of cellulose to cell walls and starch to intracellular granules is well described. CarbotraceTM680 was applied to thin tissue slices of potato, and the specimen was prepared for confocal microscopy. Using multi-laser/multi-detector analysis, image stacks of the medullary parenchyma were collected. When exciting the tissue at 535 nm and 635 nm, the optical settings specific for CarbotraceTM680 based cellulose detection, 3D projections of the image stack revealed strong yellow–red fluorescence delineating the large multi-faced cell walls of parenchyma cells (Fig. 4). Anatomically, the fluorescence signals located cellulose to cell walls as expected. This staining technique also provided details of the surface textures of the cell wall, and visualised the presence of numerous plasmodesmata.

Next, we excited the same tissue at 473 nm and 535 nm, the settings specific for starch detection. The generated 3D projection revealed strong green–yellow globular fluorescence, which located starch to the intracellular granules (Fig. 4, Video S2 in the Supporting Information). Further anatomical details could be observed, in that the granules were packed in dense clusters within the parenchyma cells, and that they showed great variation in shapes and sizes.

Taken together, our imaging experiments show that the D–A–D type electronic structure of CarbotraceTM680 makes this optotracer an extremely versatile fluorescence reporter. By simultaneously probing for multiple glucans, we are able to produce a 'carbohydrate anatomical map', which defines the physical location of glucans at sub-cellular level in native plant tissues. The ability to stain plant materials while maintaining the tissue architecture expands our recently proposed concept of analytical imaging,^[9] wherein the optical spectrum of a given pixel in the

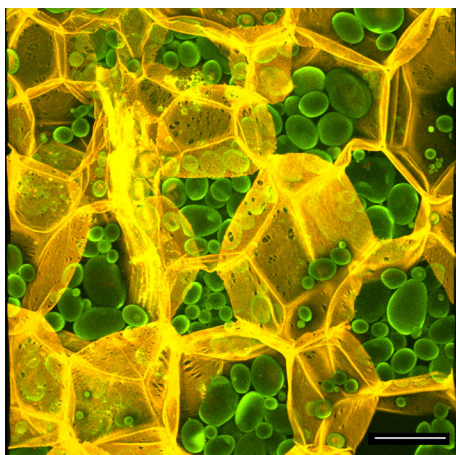


Fig. 4 Non-disruptive visualization and discrimination of starch and cellulose by multi-carbohydrate anatomical mapping in potato tissue. Micrograph of a thin slice of potato stained by CarbotraceTM680 reveal the anatomical location of cellulose and starch in the tissue. Multi-laser/multi-detector analysis shows that cellulose (pseudo-coloured in yellow) locates to the cell walls of the large, multi-faced parenchyma cells, where structural features such as plasmodesmata and small intercellular pores are clearly observed. Starch (pseudo-coloured in green) locates to intracellular granules, whose size and number per cell varies greatly. The contrast between a strongly fluorescent periphery and less intense inner core indicates incomplete penetration of CarbotraceTM680 to the dense inner compartments of the granules. The micrograph represents 3D brightest point projections of image stacks (25.52 μm stack, z-step = 1.16 μm) collected by confocal microscopy. Scale bar = 100 μm . An animation of this image stack is found as Video S2 in the Supporting Information

tissue under investigation is used to identify the nature of the chemical constituent in that location.

Conclusions

Optotracing is a novel, versatile method for non-disruptive analysis of glucose polysaccharides in solution and when present in their native location in tissues. By chemical optimization of tailor designed optotracers, we created small molecules acting as superior ligands for the detection of glucans. Short length oligomers have increased access to binding sites, to which each interaction emits its own unique spectral property. As the multiple spectral signals contribute to a wider variety of unique optical signatures, the range of detectable glucans is expanded. The spectral separation of bound optotracers was enhanced by the D–A–D-type electronic

structure of CarbotraceTM680, compared to the oligothiophene analogue. This chemically improved molecule showed extremely high selectivity to the molecular interactions, allowing minimal changes in the glucan structure, here shown as the stereochemistry, to be readily identified. Exemplified by kinetic recordings of thermo-induced swelling of starch, and multiple carbohydrate anatomical mapping in plant tissues, optotracing will likely contribute to better understanding of the chemical constituents in biomass and their processing, enabling a more efficient and targeted utilization of biomass feedstock in biorefineries, and spurring the push towards a circular economy.

Acknowledgments This work was supported by Carl Bennet AB (A.R.D.), the Erling-Persson Family Foundation and the Swedish Foundation for Strategic Research (A.R.D. and K.P.R.N.) and the Swedish Research Council (K.P.R.N.).

Open Access This article is distributed under the terms of the Creative Commons Attribution 4.0 International License (<http://creativecommons.org/licenses/by/4.0/>), which permits unrestricted use, distribution, and reproduction in any medium, provided you give appropriate credit to the original author(s) and the source, provide a link to the Creative Commons license, and indicate if changes were made.

References

- Bäck M, Appelqvist H, LeVine H 3rd, Nilsson KP (2016) Anionic oligothiophenes compete for binding of X-24 but not PIB to recombinant A β amyloid fibrils and Alzheimer's disease brain-derived A β . *Chemistry* 19:18335–18338
- Barnette AL, Bradley LC, Veres BD, Schreiner EP, Park YB, Park J, Park S, Kim SH (2011) Selective detection of crystalline cellulose in plant cell walls with sum-frequency-generation (SFG) vibration spectroscopy. *Biomacromolecules* 12:2434–2439
- Beaujuge PM, Amb CM, Reynolds JR (2010) Spectral engineering in π -conjugated polymers with intramolecular donor–acceptor interactions. *Acc Chem Res* 43:1396–1407
- Biermann CJ (1996) Kraft spent liquor recovery, and bleaching and pulp properties calculations. In: Biermann CJ (ed) *Handbook of pulping and papermaking*. Academic Press, pp 101–122, 379
- Choong FX, Bäck M, Fahlen S, Johansson LB, Melican K, Rhen M, Nilsson KPR, Richter-Dahlfors A (2016a) Real-time optotracing of curli and cellulose in live *Salmonella* biofilms using luminescent oligothiophenes. *NPJ Biofilms Microbiomes* 2:16024
- Choong FX, Bäck M, Steiner SE, Melican K, Nilsson KPR, Edlund U, Richter-Dahlfors A (2016b) Nondestructive, real-time determination and visualization of cellulose,

- hemicellulose and lignin by luminescent oligothiophenes. *Sci Rep* 6:35578
- Choong FX, Bäck M, Schulz A, Nilsson KPR, Edlund U, Richter-Dahlfors A (2018) Stereochemical identification of glucans by oligothiophenes enables cellulose anatomical mapping in plant tissues. *Sci Rep* 8:3108
- Galkin MV, Francesco DD, Edlund E, Samec JSM (2017) Sustainable sources need reliable standards. *Faraday Discuss* 202:281–301
- Heinsoo K (2017) in Europe is the Swedish Forest Industries' Main Market 2017 (Ed.: K. Heinsoo). Skogsindustrierna
- Isogai A, Saito T, Fukuzumi H (2011) TEMPO-oxidized cellulose nanofibers. *Nanoscale* 3:71–85
- Klingstedt T, Aslund A, Simon RA, Johansson LB, Mason JJ, Nystrom S, Hammarstrom P, Nilsson KPR (2011) Synthesis of a library of oligothiophenes and their utilization as fluorescent ligands for spectral assignment of protein aggregates. *Org Biomol Chem* 9:8356–8370
- Saito T, Kimura S, Nishiyama Y, Isogai A (2007) Cellulose nanofibers prepared by TEMPO-mediated oxidation of native cellulose. *Biomacromolecules* 8:2485–2491
- Sheskey PJ, Cook WG, Cable CG (2017) Handbook of pharmaceutical excipients, 8th Revised ed. Pharmaceutical Press
- Shirani H, Linares M, Sigurdson CJ, Lindgren M, Norman P, Nilsson KPR (2015) A palette of fluorescent thiophene-based ligands for the identification of protein aggregates. *Chemistry* 21:15133–15137
- Shirani H, Appelqvist H, Bäck M, Klingstedt T, Cairns NJ, Nilsson KPR (2017) Synthesis of thiophene-based optical ligands that selectively detect tau pathology in Alzheimer's disease. *Chem Eur J* 23:17127–17135
- Tasneem M, Siddique F, Ahmad A, Farooq U (2014) Stabilizers: indispensable substances in dairy products of high rheology. *Crit Rev Food Sci Nutr* 54:869–879
- Wang Q, Hu X, Du Y, Kennedy JF (2010) Alginate/starch blend fibers and their properties for drug controlled release. *Carbohydr Polym* 82:842–847
- Publisher's Note** Springer Nature remains neutral with regard to jurisdictional claims in published maps and institutional affiliations.